Clay Minerals (2025), **60**, 273–284
doi:10.1180/clm.2025.10015

Article

Iron mining waste as a sustainable material for producing bricks: microstructure, mechanical and thermal properties

Hadjer Bouzeriba[1], Nedjima Bouzidi[1], Abdelaziz Idres[2], Imen Laala[1] and Farid Ait Merzeg[1,3]

[1]Department of Mines and Geology, Laboratory of Materials Technology and Process Engineering (LTMGP), Faculty of Technology, University of Bejaia, Bejaia, Algeria; [2]Laboratory of Mineral Resources Valorization and Environment (LAVAMINE), Faculty of Earth Sciences, University of Badji Mokhtar, Annaba, Algeria and [3]Technical Platform for Physico-chemical Analysis (CRAPC-Bejaia), Bejaia, Algeria

Abstract

Iron mining waste is produced from the iron ore mining operations of El Ouenza Mine (north-east Algeria), and it is not currently recycled to preserve the environment. The current study aims at developing sustainable clay bricks by mixing clay with different proportions of iron mining waste (ranging from 10 to 50 wt.%) and fired at 850°C and 950°C. Addition of 30 wt.% Iron mining waste had a positive effect on the physical and mechanical properties of the fired clay bricks. Linear shrinkage, water absorption and porosity were reduced, while compressive and flexural strengths were increased. Furthermore, up to 30 wt.% of iron mining waste addition to the mixtures improved compressive and flexural strengths to 59.17 and 10.06 MPa, respectively, when the bricks were fired at 950°C. According to their thermal conductivity, the bricks with 10–50 wt.% iron mining waste are considered as thermal insulators, with thermal conductivity values ranging from 0.45 to 0.56 W m^{-1} K^{-1}. Adding 30 wt.% of iron mining waste can lead to the production of eco-friendly bricks with high mechanical and thermal properties, generating economic and environmental benefits.

Keywords: Clay bricks; El Ouenza Mine; environment; iron mining waste; mechanical properties; thermal conductivity

(Received 13 March 2025; revised 30 August 2025; accepted 24 September 2025; Associate Editor: Michele Dondi)

The need to build new infrastructure has contributed to the increased use of building materials due to rapid urban expansion, industrialization and development of countries (Idrees *et al.*, 2023). The manufacturing of construction materials, including cement, concrete, bricks and ceramic tiles, is a pivotal sector that is significant for national economies (Xin *et al.*, 2023a). Over the last few decades, bricks have become one of the most popular building materials used throughout the world (Weishi *et al.*, 2018). Generally, two main types of bricks are manufactured commercially: one based on cement and the other on clay (Ozturk *et al.*, 2019).

Clay masonry bricks are among the oldest and most widely used construction materials, with a rich historical background (Bai *et al.*, 2023), as the first clay brick was used as early as 4500 BCE (Rashid *et al.*, 2019; Shi *et al.*, 2023). Bricks are among the most commonly utilized construction materials due to their utility, superior strength, reduced manufacturing costs, enhanced fire resistance, durability against chemical exposure, corrosion and exposure to freeze–thaw cycles, longevity and ease of production (Dabaieh *et al.*, 2020; Hafez *et al.*, 2022). The manufacturing process for clay bricks involves extracting, crushing and mixing the raw materials and moulding them by pressing or extrusion. Once the bricks have taken shape, they are dried and fired in a kiln at high temperatures (~1200°C; Xin *et al.*, 2023b). During firing, the combination of SiO_2 and Al_2O_3 with other components of the clay contributes to the establishment of connections that give these bricks their distinctive strength and durability (Phonphuak *et al.*, 2016). The manufacture of fired bricks is linked to considerable environmental consequences, including the exhaustion of raw materials and the release of greenhouse gases, environmental degradation and ecosystem disruption (Raut & Gomez, 2017; Rashid *et al.*, 2020).

In this respect, several countries around the world have limited their use of raw materials such as clay (Sutcu *et al.*, 2016). In this context, the construction sector has developed concepts regarding sustainability to minimize the depletion of raw materials (Božič *et al.*, 2023). Utilizing several waste materials in the manufacturing of fired bricks can effectively mitigate substantial quantities of waste generated by various industrial processes, partially or totally replacing clays (Dos Reis *et al.*, 2020; Slimanou *et al.*, 2020). Several synthesis studies have been conducted to examine the application of diverse waste materials in brick manufacture, including fly ash and bottom ash (Sutcu *et al.*, 2019), dredging sediments (Slimanou *et al.*, 2020; Thomas *et al.*, 2021), glass waste (Phonphuak *et al.*, 2016), sewage sludge (Detho *et al.*, 2024), diatomite from the vegetable oil refining and brewing industries (Galán-Arboledas *et al.*, 2017), agricultural biomass wastes (Maafa *et al.*, 2023), marble waste (Sutcu *et al.*, 2015), iron ore residues (Li *et al.*, 2019; Vilela., 2020; da Silva Ramos *et al.*, 2024) and phosphate sludge (Ettoumi *et al.*, 2021).

Corresponding author: Nedjima Bouzidi; Email: nedjmabouzidi@yahoo.fr

Cite this article: Bouzeriba H, Bouzidi N, Idres A, Laala I and Ait Merzeg F (2025) Iron mining waste as a sustainable material for producing bricks: microstructure, mechanical and thermal properties. *Clay Minerals* **60**, 273–284. https://doi.org/10.1180/clm.2025.10015

© The Author(s), 2025. Published by Cambridge University Press on behalf of The Mineralogical Society of the United Kingdom and Ireland.

Iron mining waste (IMW) refers to the solid byproducts produced during the mining or processing of iron ore (Thejas & Hossiney, 2022). The chemical composition of IMW mainly consists of SiO_2, Al_2O_3, Fe_2O_3 and CaO, similar to that of natural clay, and IMW may serve as a raw material for the production of construction materials (Yang *et al.*, 2014; Weishi *et al.*, 2018). The integration of IMW in brick manufacturing is considered to be non-hazardous and to pose no environmental risk. Its use has improved brick properties such as density, porosity, water absorption and mechanical strength and reduced brick linear shrinkage (Thejas & Hossiney, 2022).

In Algeria, mining of El Ouenza iron ore significantly contributes to the country's economy, with this ore having an average iron content of 50 wt.%. El Ouenza Mine (Tebessa, Algeria) is the main supplier of iron ore to El Hadjar steel complex for the production of steel and other metals (Boutarfa *et al.*, 2023). During iron ore beneficiation, El Ouenza Mine generates large quantities of waste, estimated at 11 Mt of mine rejects after 36 Mt of iron ore is extracted (Mine Documentation, 2024). Recent studies investigated the valorisation of the IMW produced by several separation techniques, aiming at elimination of hazardous elements and enrichment of iron. The separation techniques included magnetic separation (Bouzeriba *et al.*, 2025), radiometric separation (Baala *et al.*, 2018) and electrostatic separation (Idres *et al.*, 2016). As of today, recycling of these wastes (waste rocks, IMW, limestone and low-grade iron ore) has not been carried out in Algeria. These wastes are stored in piles or tailings near the mining site; this could lead to negative impacts on human health, environmental destruction, water pollution, social problems and air pollution (Zhang *et al.*, 2021).

In this study, for the first time, the applicability of one of these wastes – IMW from iron ore mining operations at El Ouenza Mine – was investigated for the production of clay bricks. The aim of this study is to evaluate the physical, mechanical, structural, thermal and environmental properties of fired bricks incorporating IMW as the main additive. The bricks obtained by mixing clay and different amounts of IMW (0, 10, 20, 30, 40 and 50 wt.%) were dried and fired at 850°C and 950°C. The effects of physical properties, including density, porosity, water absorption and shrinkage, on mechanical strengths and thermal conductivity were also explored.

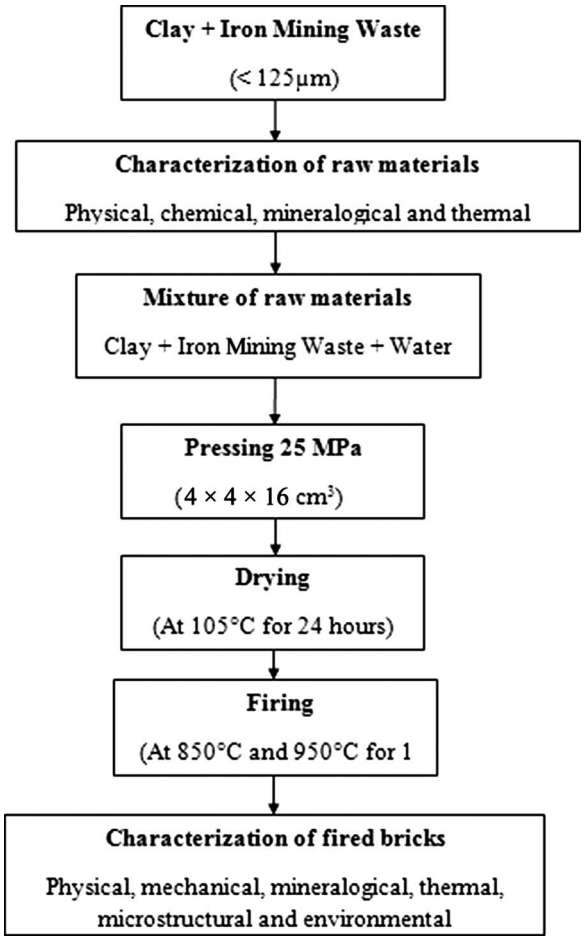


Figure 1. Simplified diagram illustrating the manufacture of bricks.

Materials and methods

Materials

Approximately 20 kg of clay was collected from the Bouteldja region (19 km from El Taref province) in north-east Algeria for use in brick making. In addition, 25 kg of IMW from iron ore mining operations was taken from the stock of landfill sites on level 845 near the mining site. Before analysis, the raw materials were dried at 105°C for 24 h, homogenized, crushed, ground and sieved to 125 µm. The bricks made from the mixing of IMW and clay were produced using the laboratory's pilot procedures and equipment. The mixtures were prepared by adding 10, 20, 30, 40 or 50 wt.% of IMW, and these were labelled MB10, MB20, MB30, MB40 and MB50, respectively. Clay bricks without IMW were produced as reference specimens (MB0; Fig. 1).

Methods

The plasticity index (PI) of the raw materials was assessed using the Atterberg limit test in accordance with the ASTM D4318-17e1 standard (Ravisankar *et al.*, 2010). Samples for liquid limit (LL) and plastic limit (PL) testing were sieved to 400 µm. The chemical compositions of the IMW and the clay were determined using X-ray fluorescence (XRF) spectroscopy with a S8 Tiger Bruker XRF spectrometer using the pressed pellet method. The mineralogical compositions of the raw materials and fired bricks were identified using X-ray diffraction (XRD) with a PANalytical advanced diffractometer (EMPYREAN) with a Cu anticathode ($\lambda = 1.54186$ Å) in the scanning range 8–55°2θ, with step size of 0.017°. The *X'Pert High Score Plus* software was used to identify the mineral species. The mineralogical compositions (wt.%) of the two raw materials were estimated according to the mass fraction of the identified phases using the reference intensity ratio values from the database selected for the qualitative identification. Thermogravimetric analysis (TGA)/differential scanning calorimetry (DSC) of the raw materials was carried out with a Perkin Elmer analyser (STA8000) operating under air flow and at a heating rate of 10°C min^{-1} from ambient temperature to 1100°C.

The mixtures were mechanically mixed in a planetary mixer for 5 min to obtain a homogeneous mixture. The samples were then mixed progressively with ~15–20 wt.% water (Idrees *et al.*, 2023) to obtain adequate plasticity without defects such as cracks and to ensure complete homogenization. The semi-dry mixes were pressed in a $4 \times 4 \times 16$ cm^3 mould under a pressure of 20 MPa using a hydraulic press (Yang *et al.*, 2014). The test mould was sprayed with oil to prevent any impact of the inner mould wall on the sample (Ravisankar *et al.*, 2010). The formed samples remained at room temperature for 24 h after extraction from the moulds, followed by

https://doi.org/10.1180/clm.2025.10015 Published online by Cambridge University Press

drying at 105°C for 24 h to yield dry bricks (Lamani *et al.*, 2017). The dried bricks were fired in an electric muffle kiln (Nabertherm) at a heating rate of 3°C min^{-1} to target temperatures of 850°C and 950°C and maintained for 1 h at the specified firing temperature to achieve greater strength. After firing, the bricks were cooled to ambient temperature through natural air convection within the kiln.

The physical and mechanical properties of the bricks were assessed in relation to ASTM construction standards for bricks. Total linear shrinkage was evaluated by directly measuring the sample pre- and post-curing length, employing a vernier calliper to ascertain the length of the samples before and after firing, in compliance with ASTM C531. The apparent density, porosity and water absorption of the fired bricks were assessed using ASTM C20 (Lang *et al.*, 2020). The compressive strength test was conducted on all brick samples following ASTM C67 (Ahmad *et al.*, 2017), utilizing a hydraulic compression machine (BeraTest) with a maximum load capacity of 2000 kN at a loading rate of 0.5 kN s^{-1}. The load was applied constantly to the samples until failure occurred. The flexural strengths of the various fired bricks were assessed per ASTM C67 (Ahmad *et al.*, 2017) using a three-point bending method with a 10 mm span between the support knife edges. This was conducted using a BeraTest mechanical testing machine, which has a maximum capacity of 150 kN, at a loading rate of 0.5 kN s^{-1} until failure occurred. Fourier-transform infrared (FTIR) analysis was performed using the KBr pellet technique by thoroughly mixing 2 mg of the materials with 100 mg of KBr *via* grinding in an agate mortar and then placing the mixtures in a press to obtain discs under high pressure using an appropriate dye. The FTIR spectra for all materials were obtained within the range of 4000–400 cm^{-1} using a Thermo Scientific iS5 series FTIR spectrometer. Scanning electron microscopy (SEM) was employed to examine the microstructures of the fired bricks utilizing an FEI QUANTA 250 model scanning electron microscope operating at 25 kV, equipped with an energy-dispersive spectroscopy (EDS) analyser.

The thermal conductivities of the bricks were determined using a conductivity temperature (CT) meter according to the NF EN ISO 8894-1 2010 standard (Gueffaf *et al.*, 2020). The heating duration for each measurement was ~300 s. Each result represent the mean of three measurements conducted on each sample.

Environmental assessment involved evaluating the mobility of contaminants using the toxicity characteristic leaching procedure (TCLP). The brick samples were pulverized and sieved through a 9.5 mm sieve to acquire a representative sample for testing. Subsequently, the extraction solution was defined by examining the pH of the sample at a 1:20 solid:liquid ratio. The extraction fluid for 1 L comprised 5.7 mL of acetic acid and water, with the pH having been previously established. The tested pH levels were 2.88 and 4.93. The samples were contained in sealed vials and agitated for 18 ± 2 h in a rotary shaker at a velocity of 30 rpm. The leachates were further filtered (0.45 µm), acidified and analysed by atomic absorption spectroscopy (AAS; PerkinElmer PinAAcle 900T; Gencel *et al.*, 2020).

Results and discussion

Characterization of the raw materials

Chemical and mineralogical composition of the raw materials

The clay is mainly composed of SiO_2 (53.72%), Al_2O_3 (23.46%) and appreciable quantities of Fe_2O_3 (5.73%; Table 1). The SiO_2 content varies generally between 45% and 60% for the clay bricks, being one of the main components of bricks (Semiz *et al.*, 2017). The Fe_2O_3, CaO, K_2O and Na_2O act as effective fluxes, reducing the temperature required to form a vitreous material in the body of the bricks as well as lowering the melting point of the clay (Ravisankar *et al.*, 2010). The clay is considered to be non-calcareous with low refractory properties (Benahsina *et al.*, 2021).

Table 1. Chemical and mineralogical compositions (wt.%) of the IMW and clay materials.

Oxide	IMW	Clay
SiO_2	49.29	53.72
Al_2O_3	9.31	23.46
Fe_2O_3	14.67	5.73
CaO	10.06	1.34
MgO	0.53	1.51
K_2O	1.14	2.65
Na_2O	0.13	0.25
MnO	0.97	0.31
TiO_2	0.15	0.67
LOI	13.75	10.36
Kaolinite	16	43
Illite	13	20
Quartz	23	15
Calcite	24	3
Dolomite	3	4
Orthose	0	5
Goethite	16	4
Hematite	3	2
Organic matter	–	2

The IMW has SiO_2, Al_2O_3, Fe_2O_3 and CaO contents of 49.29, 9.31, 14.67 and 10.06 wt.%, respectively, being comparable to those of the clay (Table 1). The high Fe_2O_3 content is responsible for the dark colour of the IMW (Muñoz *et al.*, 2016) before and after firing. MgO, TiO_2 and Na_2O are present in minor amounts. The most significant difference between clay and IMW is the loss on ignition (LOI): the LOI of IMW (13.75 wt.%) is higher than that of the clay (10.36 wt.%) due to the presence of abundant carbonates, iron oxy-hydroxides and organic matter. The inclusion of organic matter in a specific quantity is advantageous in terms of it improving the plasticity of the mixture (Achik *et al.*, 2021).

Mineralogical analysis of the two materials (Fig. 2 & Table 1) showed that the IMW contains mainly quartz (23 wt.%), kaolinite (16 wt.%), illite (13 wt.%), calcite (24 wt.%), goethite (16 wt.%), dolomite (3 wt.%) and hematite (3 wt.%). The clay is mainly composed of kaolinite (43 wt.%), illite (20 wt.%), quartz (15 wt.%), orthoclase (5 wt.%), calcite (3 wt.%), dolomite (4 wt.%) and goethite (4 wt.%).

Atterberg's limits of the raw materials

The PL is much higher for the IMW sample than for the clay sample (Table 2). This could be due to the fact that IMW is richer in fine particles (Gencel *et al.*, 2020; Gueffaf *et al.*, 2020). However, the clay sample exhibited a PI value higher than that of the IMW sample (Table 2); the latter is considered to be a medium plastic material that requires less water to become plastic. Compared to the standard index (ASTM D4318-17e1), IMW is characterized as of medium plasticity.

Thermal behaviour of the raw materials (TGA/DSC)

The thermal behaviour of the IMW sample (Fig. 3a) shows mass losses of 1.0 and 2.5 wt.% at 25–100°C and 250–300°C, respectively; these mass losses are attributed, respectively, to the loss of moisture

https://doi.org/10.1180/clm.2025.10015 Published online by Cambridge University Press

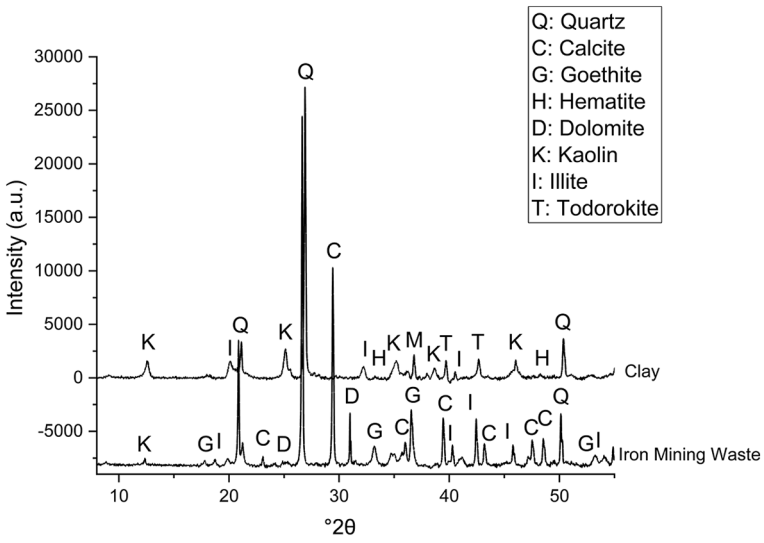


Figure 2. XRD traces of the raw materials.

Table 2. Atterberg's limits of the raw materials.

Atterbeg's limit	Clay	IMW
PL (%)	25.70	31.86
PI (%)	26.03	17.16
LL (%)	51.73	49.02

and to the dehydration of the goethite phase (α-FeO(OH)), seen as an endothermic peak centred at 274°C (Rizov, 2012). Moreover, a mass loss of 1.2 wt.% was recorded at ~490°C, seen as a weak endothermic peak ascribed to the dehydroxylation of kaolinite and illite. Finally, the mass loss of 9 wt.%, associated with an endothermic peak at 783°C, is attributed to the decomposition of carbonates.

The clay displays a mass loss of 1% at 25–100°C (Fig. 3b), with an endothermic peak centred at ~70°C, attributed to the loss of moisture. Furthermore, a mass loss of 1.7 wt.% at ~320°C can probably be attributed to the combustion of organic matter. The dehydroxylation of kaolinite and illite was recorded by an endothermic peak centred at 513°C, with a 7.5 wt.% mass loss (Mendes *et al.*, 2019). Finally, a weak exothermic peak is observed at 900–910°C, attributed to structural reorganization of metakaolinite (Slimanou *et al.*, 2020). The total mass losses from 25°C to 1000°C are 13.7 and 10.2 wt.% for the IMW and the clay, respectively.

Physicochemical characterization of the bricks

Physical characteristics of the bricks

The bricks obtained with various IMW additions fired at 850°C and 950°C show no defects such as cracks, efflorescence or swelling. However, with increasing IMW content, the colour of the bricks becomes darker. For samples MB40 and MB50, the red to brown colour of the products fired at temperatures of 850°C and 950°C is due to the high iron oxide content, which is known to be red pigment, in addition to the oxidation of Fe^{2+} to Fe^{3+}. Additionally, although the MnO content is low (~1 wt.%) in the IMW (Table 2), it is sufficient to modify the colour of the brick, producing brown to black hues and improving the surface texture by reducing roughness (Bautista-Marín *et al.*, 2021).

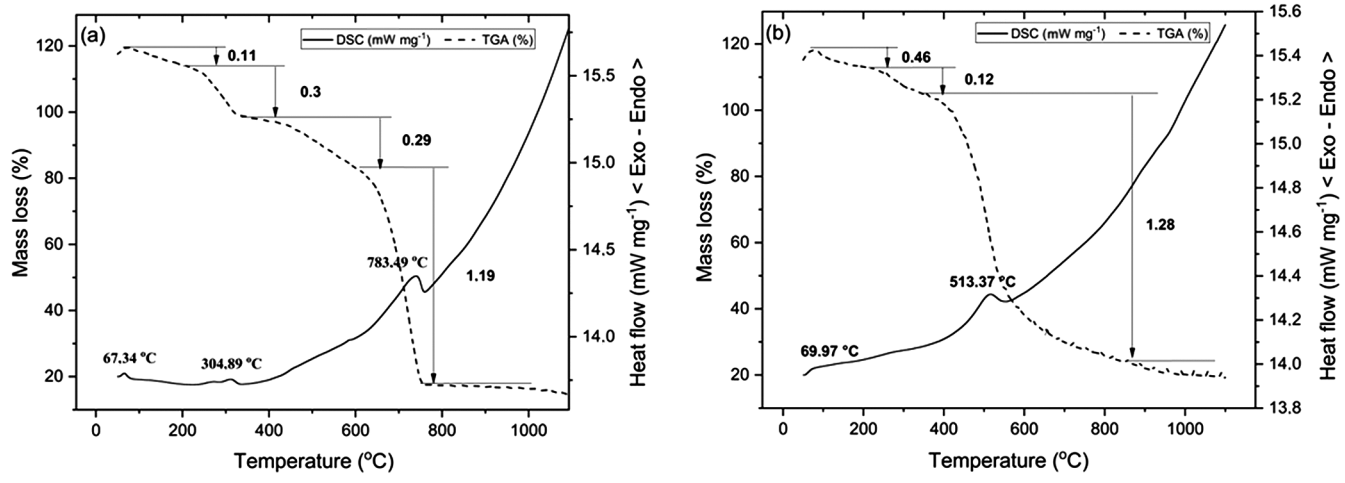


Figure 3. TGA and DSC curves of the raw materials: (a) IMW and (b) clay.

https://doi.org/10.1180/clm.2025.10015 Published online by Cambridge University Press

Table 3. Physical properties of the bricks fired at 850°C and 950 °C.

Brick	Temperature (°C)	Total linear shrinkage	Apparent porosity (%)	Bulk density (g cm^{-3})	Water absorption (%)	Compressive strength (MPa)	Flexural strength (MPa)
MB0	850	6.95 ± 0.76	36.32 ± 1.18	1.73 ± 1.90	17.51 ± 0.46	25.95 ± 0.58	1.36 ± 0.16
	950	7.32 ± 0.58	35.14 ± 0.92	1.76 ± 0.96	16.13 ± 0.11	27.53 ± 0.42	3.28 ± 0.10
MB10	850	6.42 ± 0.79	33.45 ± 1.30	1.80 ± 1.32	16.79 ± 0.95	33.20 ± 0.40	2.39 ± 0.54
	950	7.83 ± 0.41	32.27 ± 2.15	1.82 ± 1.58	15.69 ± 0.90	35.17 ± 0.48	2.73 ± 0.25
MB20	850	5.08 ± 0.82	25.20 ± 0.60	1.87 ± 1.20	13.19 ± 0.39	30.53 ± 0.48	4.58 ± 0.24
	950	6.62 ± 0.38	23.07 ± 0.95	1.89 ± 1.08	12.28 ± 0.37	32.43 ± 1.51	5.37 ± 0.31
MB30	850	4.15 ± 0.41	18.85 ± 0.87	2.07 ± 1.73	10.82 ± 0.86	51.84 ± 0.64	7.13 ± 0.22
	950	4.92 ± 0.79	18.04 ± 0.77	2.26 ± 1.40	10.14 ± 0.73	59.17 ± 0.52	10.06 ± 0.11
MB40	850	5.32 ± 0.50	26.51 ± 0.49	1.86 ± 1.89	14.34 ± 0.15	32.11 ± 0.57	5.96 ± 0.23
	950	5.87 ± 0.56	19.20 ± 0.97	2.03 ± 1.03	11.61 ± 0.92	37.58 ± 0.69	8.09 ± 0.28
MB50	850	7.52 ± 0.39	35.60 ± 0.68	1.74 ± 0.69	18.56 ± 0.71	30.22 ± 0.65	2.95 ± 0.21
	950	7.74 ± 0.12	33.42 ± 1.03	1.78 ± 0.85	13.21 ± 0.36	31.65 ± 0.52	5.59 ± 0.20

Total linear shrinkage reflects the contraction or expansion during the thermal treatment of the fired bricks. Contraction is primarily associated with the formation of the vitreous phase during firing, leading to densification through the filling of voids in the porous structure of the clay bricks. For standard clay bricks, linear shrinkage is below 8%, and when it is higher that this it leads to deformation of the fired bricks (Xin *et al.*, 2021; Pitak *et al.*, 2022). Total linear shrinkage (Table 3) varies from 4.15% to 7.52% and from 4.92% to 7.74% for the bricks fired at 850°C and 950°C, respectively. Moreover, it varies from 6.95% to 7.32% for the reference bricks (MB0) fired at 850°C and 950°C, respectively. This is linked to the moisture and constitution water losses existing between the clay particles and in the microstructure of the clay (Phonphuak *et al.*, 2016). However, total linear shrinkage decreased slightly with increasing amounts of IMW from 10 to 30 wt.%, to 4.15% and 4.92% at both firing temperatures (850°C and 950°C). This is due to the decrease in clay content and the increase in quartz present in the IMW. Quartz functioned as a degreasing agent in the mixture, mitigating potential contraction of the brick body. Moreover, the presence of quartz particles in the IMW decreased linear shrinkage due to the β-quartz to α-quartz transition for bricks containing less than 30 wt.% IMW.

With increasing IMW content above 30 wt.%, linear shrinkage increased from 19.20% to 33.42% and from 26.51% to 35.6% for the bricks fired at 850°C and 950°C, respectively. This is probably due to the dehydroxylation of the clay fraction (kaolinite and illite), in addition to the dehydroxylation of goethite, the collapse of the carbonate structure (calcite and dolomite) and the dissipation of gases that create pores (Mekki *et al.*, 2008).

The apparent density of the bricks fired at 950°C was higher than that of those fired at 850°C and varied as a function of the IMW additions from 1.73 to 2.07 g cm^{-3} and from 1.76 to 2.26 g cm^{-3} for the bricks fired at 850°C and 950°C, respectively (Table 3). The apparent density of the reference bricks was lower than that of those with IMW addition at both firing temperatures. Thereafter, it increased as with increasing IMW additions (up to 30 wt.%), and then it decreased for samples MB40 and MB50.

However, the presence of excessive Fe_2O_3 in addition to K_2O, Na_2O and MnO decreased the viscosity of the liquid phase filling the pores and facilitating the development of a glassy phase that occupied the pores of the fired bricks, decreasing their open porosity (Phonphuak *et al.*, 2016; Sutcu *et al.*, 2016; Baziz *et al.*, 2021) and thereby increasing their density. Thereafter, as the IMW content increased beyond 30 wt.%, the apparent density decreased at both firing temperatures, demonstrating increased water absorption and total linear shrinkage. Moreover, dehydroxylation of kaolinite, illite and goethite and the release of gases after firing formed pores and decreased the density of the fired bricks. The addition of IMW created a less homogeneous structure in which iron particles formed aggregates that increased voids, leading to greater absorption and porosity (Kandymov *et al.*, 2023).

Apparent porosity and water absorption followed similar trends for all of the bricks (Table 3). Both properties decreased with increasing temperature and IMW content up to 30 wt.%. However, there was a pronounced increase in both parameters when 40 and 50 wt.% of IMW were added to the mixtures, but these values nevertheless were lower than those of the reference bricks (MB0). The addition of 30 wt.% of IMW considerably decreased apparent porosity and water absorption to 18.04% and 10.14%, respectively, for the bricks fired at 950°C. This is due to the iron oxides (Fe_2O_3) and alkali oxides (K_2O, Na_2O), which facilitate the development of a glassy phase that occupies the pores of the fired bricks at 850°C and 950°C (Phonphuak *et al.*, 2016).

Mineralogical analysis of the fired clay bricks

The main phases of bricks fired at 850°C are quartz, hematite, gehlenite ($2CaO.Al_2O_3.SiO_2$) and anorthite (Fig. 4a); these phases increased as a function of increasing IMW addition. However, anorthite formed as a metastable solid solution from the phase transformation of calcite and aluminosilicates ($CaO–Al_2O_3–SiO_2$ system) in sample MB30 (DeCeanne *et al.*, 2022). At 950°C, quartz, hematite, gehlenite and anorthite were the main mineralogical phases of the fired bricks, but the intensities of their peaks were slightly diminished compared to bricks fired at 850°C (Fig. 4b). Moreover, the intensity of the quartz peaks of sample MB30 were decreased, whereas the intensities of the peaks of hematite, gehlenite and anorthite were increased. This might be due to the formation of a glassy phase in sample MB30, facilitated by the presence of fluxing agents. Fe_2O_3 along with K_2O and Na_2O are fluxing agents, facilitating the formation of a glassy phase at lower temperatures (Klaarenbeek, 1961; Maniatis *et al.*, 1981). When the addition of IMW exceeded 30 wt.%, the bricks fired at both temperatures (850°C and 950°C) acquired more porous structures due to the excessive clay, goethite and calcite contents, which increased water absorption, porosity and total shrinkage (Table 3). Moreover, as the amount of refractory oxides (Al_2O_3, MgO) increased, the firing temperatures used in this study became insufficient to decrease the viscosity of the liquid phase, which fills the pores and facilitates

https://doi.org/10.1180/clm.2025.10015 Published online by Cambridge University Press

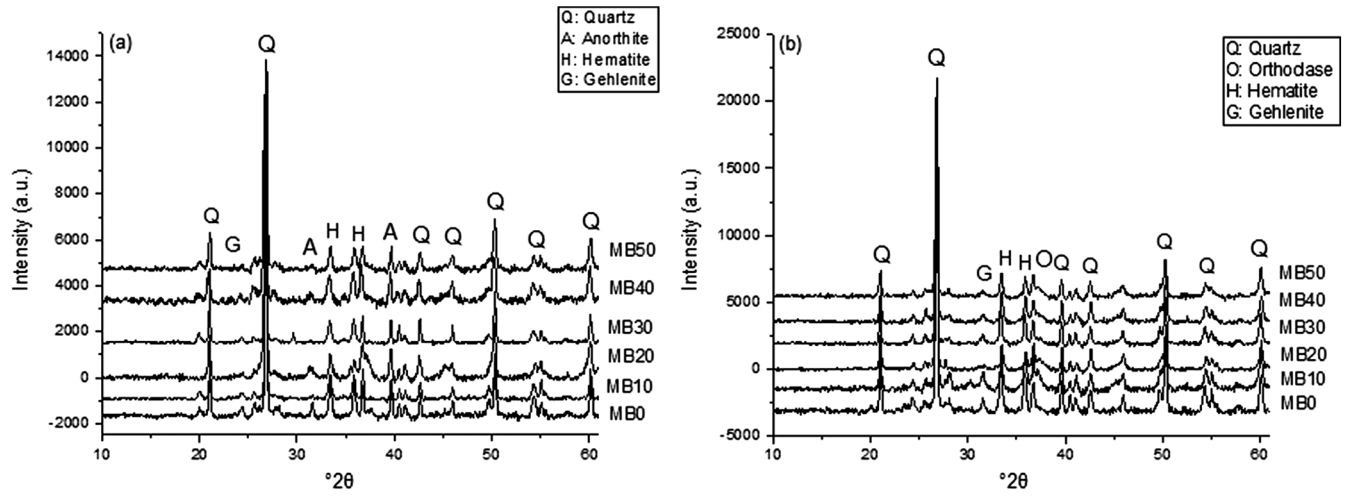


Figure 4. XRD traces of bricks fired at (a) 850°C and (b) 950°C.

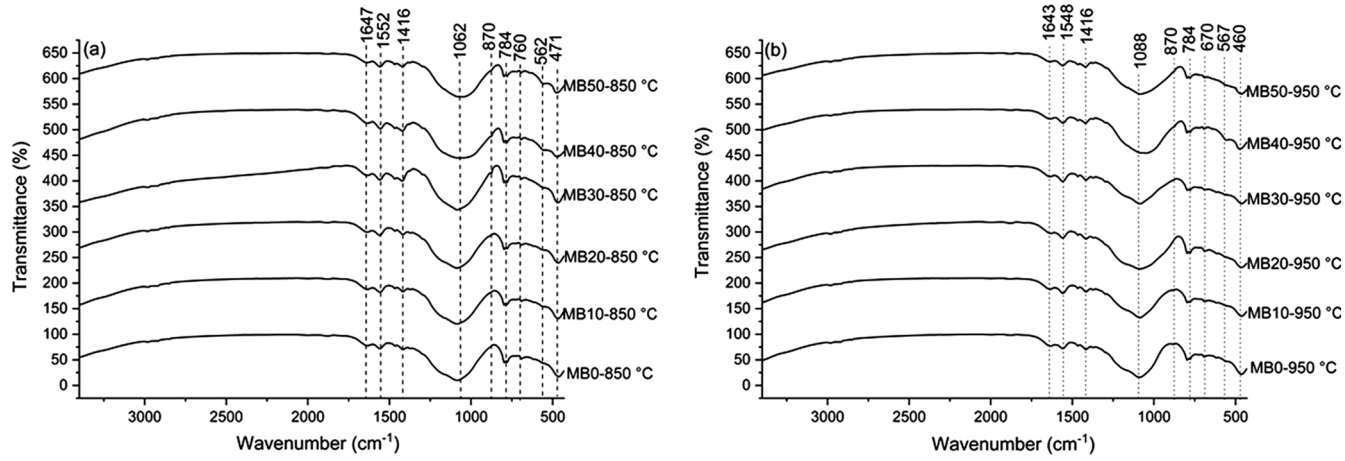


Figure 5. FTIR spectra of bricks fired at (a) 850°C and (b) 950°C.

the formation of a glassy phase that further fills the pores of the fired bricks. The peaks of quartz and hematite slightly increased in intensity in samples MB40 and MB50 when the samples were fired at 950°C.

FTIR characterization of the bricks

All of the samples show weak doublet bands at 1647 and 1552 cm^{-1} (Fig. 5a,b), attributed to bending and stretching vibrations due the presence of adsorbed water molecules (Ravisankar *et al.*, 2010). A weak band at ∼1416 cm^{-1}, characteristic of carbonates, is present in all samples fired at 850°C and 950°C. The 1062–1088 cm^{-1} absorption bands represent asymmetric Si–O stretching of the main silicate tetrahedral vibrations (Bahçeli *et al.*, 2016). The excessive broadening of absorption bands in the 1100–1000 cm^{-1} range are attributed to disorder within the tetrahedral sites, leading to the expansion of the Si–O stretching band (Ravisankar *et al.*, 2010). The weak shoulder absorption bands in the range of 916–922 cm^{-1} observed in the bricks fired at 850°C (MB30, MB40 and MB50) are due to Al–OH flexure vibrations of phyllosilicates (Terra *et al.*, 2015). These vibrations were retained in samples MB40 and MB50 fired at 950°C. Additionally, the weak shoulder at 870 cm^{-1} is observed for the MB30, MB40 and MB50 samples fired at 850°C, which is attributed to FeAlOH vibrations present in the IMW (Eliche-Quesada *et al.*, 2018). However, this shoulder band is absent from samples MB0, MB10 and MB20. On the other hand, the weak band at 870 cm^{-1} is present in samples MB40 and MB50. The weak bands observed at 784 and 760 cm^{-1} observed in all of the samples are attributed to the Si–O symmetrical stretching vibrations of quartz (Barua *et al.*, 2003; Namduri & Nasrazadani, 2008). However, the weak shoulder observed at 688 cm^{-1} in all of the samples is attributed to Si–O symmetrical bending vibrations due to Al for Si substitution. In the 550–570 cm^{-1} region, a medium-intensity band is observed in the FTIR spectra of all of the samples (except MB0 and MB10) fired at 850°C and 950°C (Fig. 5a,b). This band is ascribed to Fe–O deformation bond of hematite (Adazabra *et al.*, 2017).

Microstructure of the fired bricks

The textural characteristics and the evolution of the surface porosity with firing temperature (850°C and 950°C) were investigated using SEM. Figure 6 shows the SEM observations of the surfaces of the bricks with 0, 30 and 40 wt.% IMW fired at 850°C (MB0, MB30 and MB40, respectively). Sample MB0 exhibits high porosity (open and closed pores) and calcite and quartz particles that are not yet fused (Fig. 6a). Moreover, some agglomerates of fine particles of clay and iron particles are evidenced on the surfaces of all bricks

https://doi.org/10.1180/clm.2025.10015 Published online by Cambridge University Press

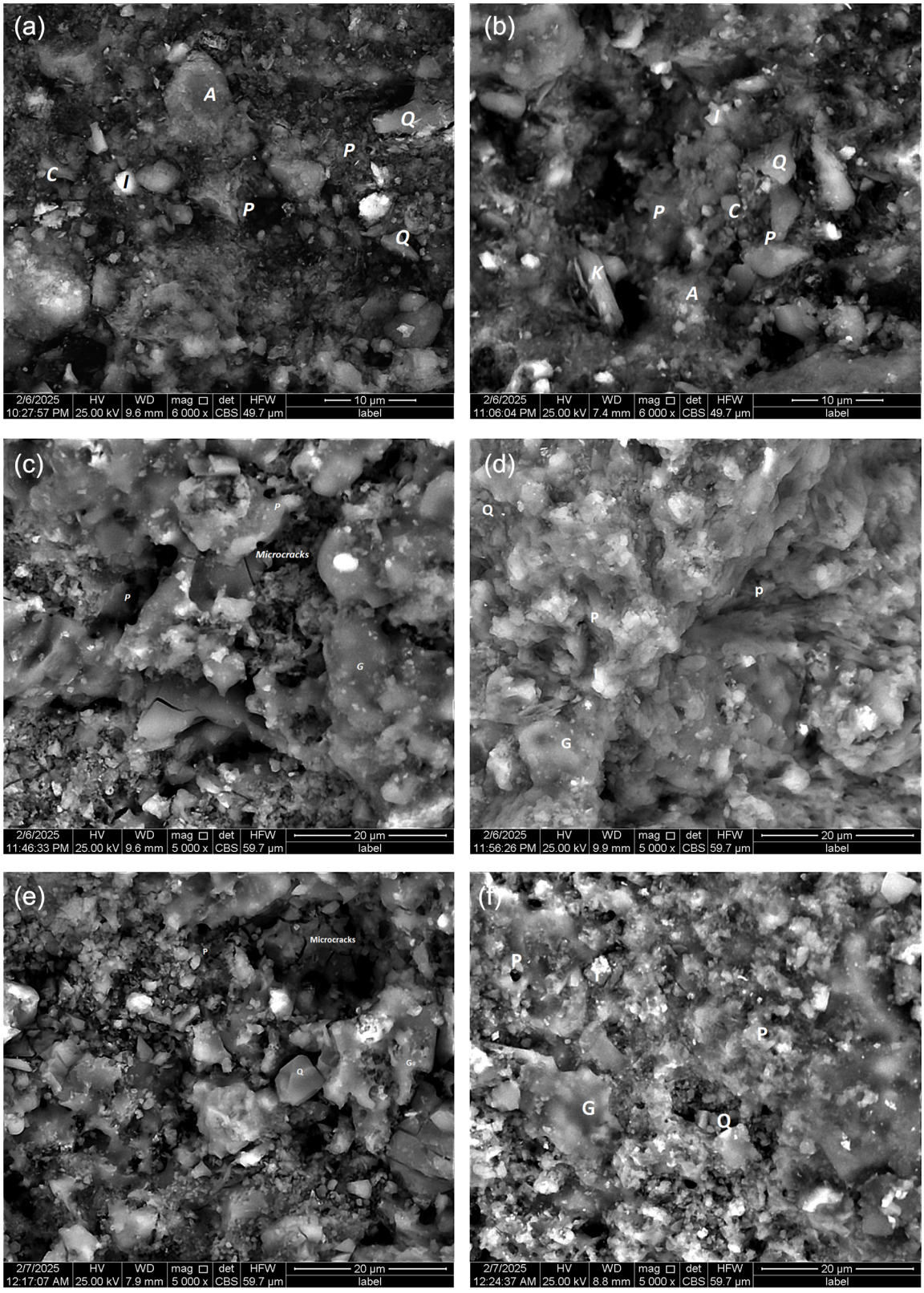


Figure 6. SEM images of the bricks fired at 850°C and 950°C: (a) MB0-850, (b) MB30-850, (c) MB40-850, (d) MB0-950, (e) MB30-950 and (f) MB40-950. A = agglomerates; C = calcite, G = glass, I = iron, K = kaolinite; P = pore, Q = quartz.

that have not experienced dehydroxylation. As the amount of the IMW increased to 30 wt.%, the morphology of the bricks changed; their structure became denser and the pores are less abundant than the MB0-850 sample (Fig. 6b). Some kaolinite, quartz and calcite particles along with agglomerates still appear in the matrix of the bricks. The microstructure of the sample containing 40 wt.%

https://doi.org/10.1180/clm.2025.10015 Published online by Cambridge University Press

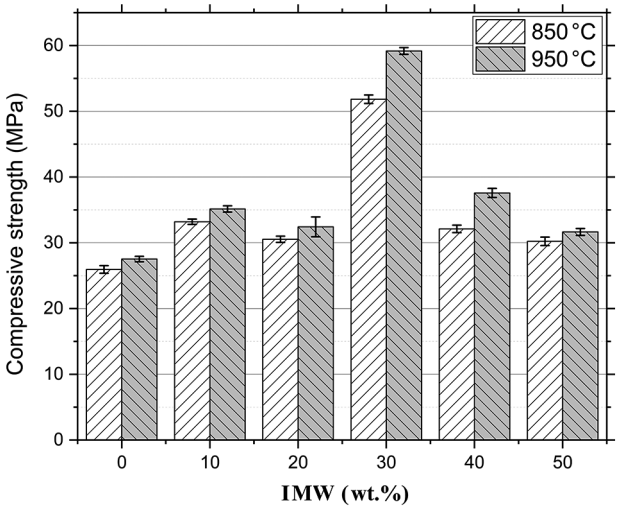


Figure 7. Compressive strength of the bricks as a function of IMW addition.

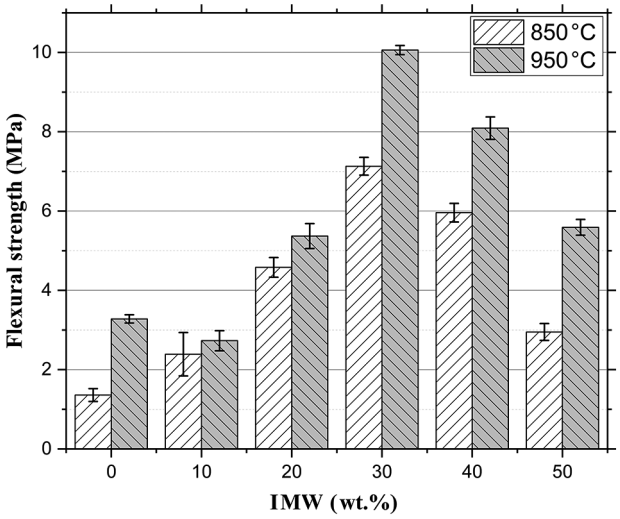


Figure 8. Flexural strength of the bricks as a function of IMW addition.

IMW (Fig. 6c) presented excessive pores and some micro-cracks due to hydration of CaO during calcination (Cultrone *et al.*, 2004); this leads to increases in porosity and total linear shrinkage and a decrease in density (Table 3).

As the sintering temperature increased to 950°C, addition of IMW modified the microstructure of the specimens, leading to densification of the bricks and reduction of porosity with a heterogeneous phase distribution and visible closed porosity (Fig. 6d–f). This process involves decreases in total linear shrinkage and open porosity, as observed in sample MB30. In all of the bricks, the mineralogical transformations were not coupled with phase consolidation (i.e. particle rearrangement and diffusion by a solid state during firing, leading to the growth of contact points during the sintering process). Moreover, the formation of interconnected grains and a glassy phase surrounding the grain boundaries is evidenced in samples MB30 and MB40. Agglomerates of particles embedded in a glassy phase are shown in Fig. 6e,f. The high Fe_2O_3 content of the waste plays a role as a fluxing agent for the mixture (Baziz *et al.*, 2021). Overall, the incorporation of large amounts of IMW (40–50 wt.%) resulted in an interlinked pore architecture, as is indicated by the water absorption data (Slimanou *et al.*, 2020).

Mechanical and thermal properties of the fired bricks

Compressive strength

The compressive strengths of the reference bricks fired at 850°C and 950°C were 25.95 ± 0.58 and 27.53 ± 0.42 MPa, respectively (Fig. 7). These values exhibited an almost linear increase with the incorporation of 30 wt.% IMW for bricks fired at 850°C and 950°C, reaching peak values of 51.84 ± 0.64 and 59.17 ± 0.52 MPa at 850°C and 950°C, respectively. This increase is due to the reduction of porosity, leading to an increase in density. Moreover, hematite and alkali oxides lowered the fusion point of the bricks and hence promoted the liquid phase cementing the crystalline phase in the matrix (James *et al.*, 1976; Sedmale *et al.*, 2006; Allegretta *et al.*, 2016).

With increasing IMW addition, the compressive strengths of the bricks decreased from 32.11 ± 0.57 to 30.22 ± 0.65 MPa and from 37.58 ± 0.69 to 31.65 ± 0.52 MPa for the bricks fired at 850°C and 950°C containing 40 and 50 wt.% IMW, respectively. This is due to the increases in water absorption (Table 3) and porosity of the bricks because of their excessive clay and quartz phase contents (Figs 4 & 5), which require higher firing temperature for sintering and consolidation (Coletti *et al.*, 2016). However, the increases in quartz and hematite contents in the bricks could negatively affect compressive strength as they could produce more heterogeneity in the structures and induce micro-cracks (Monteiro & Vieira, 2004; Souza *et al.*, 2008). Overall, the compressive strengths of all of the bricks fired at 850°C and 950°C were much higher than those of the conventional bricks, which have a minimum compressive strength of 10 MPa (Slimanou *et al.*, 2020).

Flexural strength

The construction industry considers the flexural strength of fired bricks to be the main quality factor for assessing their suitability (Semiz *et al.*, 2017). ASTM C67 requires that the flexural strength of fired bricks exceeds 2.5 MPa (Dos Reis *et al.*, 2020). In the present study, flexural strength increased as a function of IMW addition up to 30 wt.% after firing at 850°C and 950°C (Fig. 8). The reference bricks exhibited values varying from 1.36 ± 0.16 to 3.28 ± 0.10 MPa at 850°C and 950°C, respectively. The flexural strengths of the fired bricks varied from 1.36 ± 0.16 to 7.13 ± 0.22 MPa and from 3.28 ± 0.10 to 10.06 ± 0.11 MPa at 850°C and 950°C, respectively. Increasing the firing temperature led to increased flexural strength.

The optimum flexural strength was attained when the bricks contained 30 wt.% IMW (7.13 ± 0.22 and 10.06 ± 0.11 MPa at 850°C and 950°C, respectively). This is due to the improvement of vitrification and/or consolidation when the firing temperature was increased. However, at above 30 wt.% addition of IMW, the flexural strength decreased to 2.95 ± 0.21 MPa. This decline in this mechanical characteristic is attributed to porosity and water absorption increasing after the addition of such large contents of IMW.

Thermal conductivity

Materials with low thermal conductivity are superior insulators and help reduce heat loss or gain in buildings. It was therefore crucial to acquire bricks with optimal mechanical and thermal properties. Indeed, standard red bricks have a thermal conductivity of 0.6 W m^{-1} K^{-1}, whereas insulating bricks have a lower thermal conductivity of 0.15 W m^{-1} K^{-1} (Kreimeyer, 1987).

https://doi.org/10.1180/clm.2025.10015 Published online by Cambridge University Press

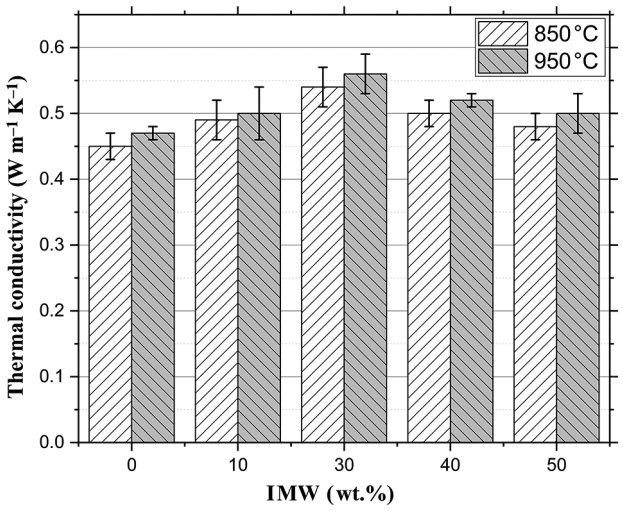


Figure 9. Thermal conductivity of the bricks as a function of IMW addition.

The thermal conductivity of the bricks fired at 850°C and 950°C increased as a function of IMW addition up to 30 wt.% (Fig. 9). The thermal conductivities of the reference bricks were 0.45 ± 0.02 and 0.47 ± 0.01 W m^{-1} K^{-1}, and the bricks with 30 wt.% IMW had slightly higher thermal conductivities of 0.54 ± 0.03 and 0.56 ± 0.03 W m^{-1} K^{-1} at 850°C and 950°C, respectively. This is attributed to the lower porosity of these bricks, which influenced their thermal properties. Addition of IMW up to 30 wt.% increased the bulk density and thermal conductivity of the bricks at both firing temperatures. Further IMW addition (40–50 wt.%) to the brick specimens caused a slight decrease of thermal conductivity and density due to increased porosity. This is attributed to air being present in pore voids, which has a low thermal conductivity (0.024 W m^{-1} K^{-1}), acting as thermal insulator (Kadir & Mohajerani, 2015; Wang *et al.*, 2024).

Environmental assessment

According to the results regarding the toxicity characteristics (i.e. TCLP) of the bricks with 0, 10, 20, 30 and 40 wt.% IMW (Table 4), the heavy metal concentrations of all of the bricks decreased with increasing firing temperature from 850°C to 950°C. The concentration of Zn and Ni is higher in the reference bricks than in the bricks with IMW, probably because the clay itself contains greater contents of Zn and Ni. However, the Pb and Fe concentrations are higher in the bricks with IMW than in the reference bricks. During firing, heavy metals are trapped and immobilized in the glassy phase composing the structure of the bricks at both firing temperatures. Overall, the results of these experiments showed heavy metal contents below the limits set by the US Environmental Protection Agency (EPA; Chen & Ma, 1998).

Summary

In this study, 30 wt.% IMW could be used as raw material to produce clay bricks; these bricks had compressive strengths of 51.84 ± 0.64 and 59.17 ± 0.52 MPa and thermal conductivities of 0.45 ± 0.01 and 0.50 ± 0.02 after firing at 850°C and 950°C, respectively. Addition of IMW reduces linear shrinkage and compressive strength during firing. Nevertheless, addition of 20 wt.% IMW is considered acceptable for maintaining quality in line with fired brick standards. Chen *et al.* (2011) showed that bricks obtained by mixing 84 wt.% IMW, 10 wt.% clay and 6 wt.% fly ash fired at 980–1030°C complied with the Chinese standard. In addition, water absorptions of 16.54–17.93% and compressive strengths of 20.03–22.92 MPa were observed, also satisfying the requirements of this standard. In conclusion, IMW offers a promising alternative in the manufacture of fired bricks, with satisfactory physical and mechanical properties and minimal environmental impact.

Conclusions

This study examined the use of as-received IMW for the production of fired clay bricks. Different proportions of IMW (10, 20, 30, 40 and 50 wt.%) were added to the bricks. Physical, mechanical and thermal properties, microstructure and environmental impact were evaluated. Based on the results of this study, the following conclusions can be drawn:

- The IMW has a high concentration of Fe_2O_3, SiO_2 and silica and contains abundant kaolinite (16%), illite (13%), quartz (23%), goethite (16%) and calcite (24%) and minor hematite (3%) and dolomite (3%).
- Total shrinkage, water absorption and porosity are significantly reduced by increasing the amount of IMW up to 30 wt.% of brick composition at both firing temperatures (850°C and 950°C). This is due to the decrease in clay content and the increase in quartz with the addition of the IMW. Brick density increased with firing temperature (950°C) and IMW addition (up to 30 wt.%) due to the formation of a liquid phase, promoted by the Fe_2O_3 content, which filled the internal pores and reduced open porosity. However, when IMW exceeded 30 wt.%, the density decreased as the open porosity and water absorption increased because the sintering temperature (950°C) was not sufficient to form a glassy phase. The water absorption of all bricks was below 20 wt.%, meeting the ASTM standard for these bricks.
- The main phases of bricks at 850°C are quartz, hematite, gehlenite and anorthite, the abundance of which increased with the addition of IMW. However, anorthite appeared as a metastable solid solution resulting from the phase transformation of calcite

Table 4. Leachability of the heavy metals as a function of temperature (concentrations in mg L^{-1}).

	Bricks fired at 850°C				Bricks fired at 950°C				
Element	MB0	MB10	MB30	MB40	MB0	MB10	MB30	MB40	US EPA limit[a]
Zn	0.718	0.515	0.382	0.361	0.541	0.367	0.366	0.340	500
Pb	2.276	3.774	4.466	4.801	1.225	1.453	2.358	2.647	5
Ni	0.164	0.127	0.109	0.092	0.114	0.108	0.068	0.043	11
Fe	354.83	393.76	414.70	401.83	173.15	239.86	264.20	314.84	–

[a]US EPA (1996).

https://doi.org/10.1180/clm.2025.10015 Published online by Cambridge University Press

and aluminosilicate phases in sample MB30. Additionally, the bricks fired at 950°C have the same phases, although these are less abundant compared to those of bricks fired at 850°C.

- All samples showed mechanical strength values in excess of the required standards, with compressive strengths of 25.95 and 27.53 MPa after firing at 850°C and 950°C, respectively. When the optimum (30 wt.%) quantity of IMW is added, the compressive and flexural strengths of the bricks increased from 51.84 to 59.17 MPa and from 7.13 to 10.06 MPa, respectively, for the bricks fired at 850°C and 950°C. This is due to densification and the elimination of open porosity. The presence of Fe_2O_3 as well as fluxing agents (Na_2O, K_2O and Mn_2O) decreases the liquid temperature, which leads to the formation of a glassy phase, as shown by the SEM images of the samples. The decline in mechanical characteristics with the incorporation of 40 and 50 wt.% IMW is attributed mostly to the greater porosity and water absorption after the addition of such quantities of IMW.
- Thermal conductivity increased with the incorporation of IMW after firing at 850°C and 950°C. Brick samples with 30 wt.% IMW showed thermal conductivity values of 0.54 and 0.56 W m^{-1} K^{-1}. The minimum thermal conductivities achieved were 0.45 and 0.47 W m^{-1} K^{-1} for the control bricks fired at 850°C and 950°C, respectively. The results of the TCLP showed that the heavy metals were trapped during firing and immobilized in the glassy phase that makes up the brick structure at both firing temperatures. The results for all samples were below US EPA limits.
- IMW can be successfully recycled and met all current standards for brick-making. In this case study, the optimum amount of IMW was 30 wt.%, giving maximum values of mechanical strength and acceptable values of thermal conductivity with less open porosity. Therefore, fired brick production in the temperature range of 850–950°C with the incorporation of IMW could represent a substantial step towards decreasing pollution and environmental impacts of this industry, which could contribute to sustainable development and circular economy principles.

Acknowledgements. The authors want to thank the Center for Scientific and Technical Research in Physico-Chemical Analysis of Bejaia, Algeria (CRAPC) for facilitating this research. We also thank El Ouenza Mine for providing us with the IMW samples.

Financial support. None.

Competing interests. The authors declare none.

References

Achik M., Benmoussa H., Oulmekki A., Ijjaali M., el Moudden N., Touache A. *et al.* (2021) Evaluation of technological properties of fired clay bricks containing pyrrhotite ash. *Construction and Building Materials*, **269**, 121312.

Adazabra A.N., Viruthagiri G. & Shanmugam N. (2017) Infrared analysis of clay bricks incorporated with spent shea waste from the shea butter industry. *Journal of Environmental Management*, **191**, 66–74.

Ahmad S., Iqbal Y. & Muhammad R. (2017) Effects of coal and wheat husk additives on the physical, thermal and mechanical properties of clay bricks. *Boletin de La Sociedad Espanola de Ceramica y Vidrio*, **56**, 131–138.

Allegretta I., Pinto D. & Eramo G. (2016) Effects of grain size on the reactivity of limestone temper in a kaolinitic clay. *Applied Clay Science*, **126**, 223–234.

Baala D., Idres A., Bounouala M. & Benselhoub A. (2018) Radiometric sorting techniques for mining wastes from Ouenza iron mine (Algeria). *Scientific Bulletin of National Mining University*, **5**, 30–38.

Bahçeli S., Güleç G., Erdołan H. & Söłüt B. (2016) Micro-Raman and FT-IR spectroscopic studies of ceramic shards excavated from ancient Stratonikeia city at Eskihisar village in west-south Turkey. *Journal of Molecular Structure*, **1106**, 316–321.

Bai M., Xiao J., Gao Q. & Shen J. (2023) Utilization of construction spoil and recycled powder in fired bricks. *Case Studies in Construction Materials*, **18**, e02024.

Barua A.G., Boruah B.R., Bhattacharyya S. & Baruah G.D. (2003) Spectroscopic investigation of the Dergaon meteorite with reference to 10 μm and 20 μm bands. *Pramana - Journal of Physics*, **60**, 47–52.

Bautista-Marín J.D., Esguerra-Arce A. & Esguerra-Arce J. (2021) Use of an industrial solid waste as a pigment in clay bricks and its effects on the mechanical properties. *Construction and Building Materials*, **306**, 124848.

Baziz A., Bouzidi N. & Eliche-Quesada D. (2021) Recycling of gold mining reject from Amesmessa mine as ceramic raw material: microstructure and mechanical properties. *Environmental Science and Pollution Research*, **28**, 46738–46747.

Benahsina A., Taha Y., Bouachera R., Elomari M. & Bennouna M.A. (2021) Manufacture and characterization of fired bricks from gold mine waste rocks. *Minerals*, **11**, 695.

Boutarfa F., Idres A., Mekti Z., Graine R., Tiour F., Dovbash N. *et al.* (2023) Airborne dust pollution emitted by El Hadjar Metallurgical Complex: quantification, characterization, and occupational health hazards. *Technology Audit and Production Reserves*, **5**, 20–28.

Bouzeriba H., Bouzidi N., Idres A., Laala I. & Zaoui L. (2025) Feasibility assessment of low-grade iron ore from El Ouenza mine by high-intensity magnetic separation. *Naukovyi Visnyk Natsionalnoho Hirnychoho Universytetu*, **1**, 28–33.

Božič M., Žibret L., Kvočka D., Pranjić A.M., Gregorc B. & Ducman V. (2023) Drava river sediment in clay brick production: characterization, properties, and environmental performance. *Journal of Building Engineering*, **71**, 106470.

Chen M. & Ma L.Q. (1998) Comparison of four USEPA digestion methods for trace metal analysis using certified and Florida soils. *Journal of Environmental Quality*, **27**, 1294–1300.

Chen Y. Zhang Y., Chen T., Zhao Y. & Bao S. (2011) Preparation of eco-friendly construction bricks from hematite tailings. *Construction and Building Materials*, **25**, 2107–2111.

Coletti C., Cultrone G., Maritan L. & Mazzoli C. (2016) How to face the new industrial challenge of compatible, sustainable brick production: study of various types of commercially available bricks. *Applied Clay Science*, **124–125**, 219–226.

Cultrone G., Sebastián E., Elert K., de la Torre M.J., Cazalla O. & Rodriguez-Navarro C. (2004) Influence of mineralogy and firing temperature on the porosity of bricks. *Journal of the European Ceramic Society*, **24**, 547–564.

da Silva Ramos L.T., de Azevedo R.C., da Silva Bezerra A.C., do Amaral L.M. & Oliveira R.D. (2024) Iron ore tailings as a new product: a review-based analysis of its potential incorporation capacity by the construction sector. *Cleaner Waste Systems*, **7**, 100137.

Dabaieh M., Heinonen J., El-Mahdy D. & Hassan D.M. (2020) A comparative study of life cycle carbon emissions and embodied energy between sun-dried bricks and fired clay bricks. *Journal of Cleaner Production*, **275**, 122998.

DeCeanne A.V., Rodrigues L.R., Wilkinson C.J., Mauro J.C. & Zanotto E.D. (2022) Examining the role of nucleating agents within glass–ceramic systems. *Journal of Non-Crystalline Solids*, **591**, 121714.

Detho A., Kadir A.A. & Ahmad S. (2024) Utilization of wastewater treatment sludge in the production of fired clay bricks: an approach towards sustainable development. *Results in Engineering*, **21**, 101708.

Dos Reis G.S., Cazacliu B.G., Cothenet A., Poullain P., Wilhelm M., Sampaio C.H. *et al.* (2020) Fabrication, microstructure, and properties of fired clay bricks using construction and demolition waste sludge as the main additive. *Journal of Cleaner Production*, **258**, 120733.

Eliche-Quesada D., Martínez-García C., Martínez-Cartas M.L., Cotes-Palomino M.T., Pérez-Villarejo L., Cruz-Pérez N. & Corpas-Iglesias F.A. (2011) The use of different forms of waste in the manufacture of ceramic bricks. *Applied Clay Science*, **52**, 270–276.

Eliche-Quesada D., Sandalio-Pérez J.A., Martínez-Martínez S., Pérez-Villarejo L. & Sánchez-Soto P.J. (2018) Investigation of use of coal fly ash in eco-friendly construction materials: fired clay bricks and silica-calcareous non fired bricks. *Ceramics International*, **44**, 4400–4412.

https://doi.org/10.1180/clm.2025.10015 Published online by Cambridge University Press

Ettoumi M., Jouini M., Neculita C.M., Bouhlel S., Coudert L., Taha Y. & Benzaazoua M. (2021) Characterization of phosphate processing sludge from Tunisian mining basin and its potential valorization in fired bricks making. *Journal of Cleaner Production*, **284**, 124750.

Fernandes F.M. (2019) Clay bricks. Pp. 3–19 in: *Long-Term Performance and Durability of Masonry Structures* (B. Ghiassi & P.B. Lourenço, editors). Woodhead Publishing, Sawston, UK.

Galán-Arboledas R.J., Cotes-Palomino M.T., Bueno S. & Martínez-García C. (2017) Evaluation of spent diatomite incorporation in clay based materials for lightweight bricks processing. *Construction and Building Materials*, **144**, 327–337.

Gencel O., Erdugmus E., Sutcu M. & Oren O.H. (2020) Effects of concrete waste on characteristics of structural fired clay bricks. *Construction and Building Materials*, **255**, 119362.

Gueffaf N., Rabehi B. & Boumchedda K. (2020) Recycling dam sediments for the elaboration of stabilized blocks. *International Journal of Engineering Research in Africa*, **50**, 131–144.

Hafez R.D.A., Tayeh B.A. & Abd-Al Ftah R.O. (2022) Development and evaluation of green fired clay bricks using industrial and agricultural wastes. *Case Studies in Construction Materials*, **17**, e01391.

Hussien A., Al Zubaidi R., Jannat N., Ghanim A., Maksoud A., Al-Shammaa A. (2024) The effects of tea waste additive on the physical and mechanical characteristics of structural unfired clay bricks. *Alexandria Engineering Journal*, **101**, 282–294.

Idrees M., Akbar A., Saeed F., Gull M. & Eldin S.M. (2023) Sustainable production of low-shrinkage fired clay bricks by utilizing waste plastic dust. *Alexandria Engineering Journal*, **68**, 405–416.

Idres A., Bouhedja A., Bounouala M. &Benselhoub A. (2016) New method of electrostatic separation of the oxidized iron ore. *Mining Science*, **23**, 33–42.

James R.S., Turnock A.C. & Fawcett J.J. (1976) The stability and phase relations of iron chlorite below 8.5 kb P-H20. *Contributions to Mineralogy and Petrology*, **56**, 1–25.

Kadir A.A. & Mohajerani A. (2015) Effect of heating rate on gas emissions and properties of fired clay bricks and fired clay bricks incorporated with cigarette butts. *Applied Clay Science*, **104**, 269–276.

Kandymov N., Korpayev S., Durdyev S., Myratberdiyev R. & Gurbanmyradova L. (2023) Manufacturing of fired clay bricks for internal walls with dolomite residue as a secondary material. *Buildings*, **13**, 3065.

Klaarenbeek F.W. (1961) The development of yellow colors in calcareous bricks. *Transactions of the British Ceramic Society*, **60**, 739–771.

Kreimeyer R. (1987) Some notes on the firing colour of clay bricks. *Applied Clay Science*, **2**, 175–183.

Lamani S.R., Mangalpady A. & Vardhan H. (2017) Investigating the utility of iron ore waste in preparing non-fired bricks. *Journal of The Institution of Engineers (India): Series D*, **98**, 239–250.

Lang L., Chen B. & Pan Y. (2020) Engineering properties evaluation of unfired sludge bricks solidified by cement–fly ash–lime admixed nano-SiO_2 under compaction forming technology. *Construction and Building Materials*, **259**, 119879.

Li R., Zhou Y., Li C., Li S. & Huang Z. (2019) Recycling of industrial waste iron tailings in porous bricks with low thermal conductivity. *Construction and Building Materials*, **213**, 43–50.

Maafa I.M., Abutaleb A., Zouli N., Zeyad A.M., Yousef A. & Ahmed M.M. (2023) Effect of agricultural biomass wastes on thermal insulation and self-cleaning of fired bricks. *Journal of Materials Research and Technology*, **24**, 4060–4073.

Maniatis Y., Simopoulos A. & Kostikas A. (1981) Moessbauer study of the effect of calcium content on iron oxide transformations in fired clays. *Journal of the American Ceramic Society*, **64**, 263–269.

Mekki H., Anderson M., Benzina M. & Ammar E. (2008) Valorization of olive mill waste water by its incorporation in building bricks. *Journal of Hazardous Materials*, **158**, 2–3.

Mendes B.C., Pedroti L.G., Fontes M.P.F., Ribeiro J.C.L., Vieira C.M.F., Pacheco A.A. & de Azevedo A.R.G. (2019) Technical and environmental assessment of the incorporation of iron ore tailings in construction clay bricks. *Construction and Building Materials*, **227**, 116669.

Mine Documentation (2024) *The El Ouenza Mine History and Future*. Study and Development Division Geology Service, El Ouenza Mine, Tebessa, Algeria.

Monteiro S.N. & Vieira C.M.F. (2004) Influence of firing temperature on the ceramic properties of clays from Campos dos Goytacazes, Brazil. *Applied Clay Science*, **27**, 3–4.

Muñoz V.P., Morales O.M.P., Letelier G.V. & Mendívil G.M.A. (2016) Fired clay bricks made by adding wastes: Assessment of the impact on physical, mechanical and thermal properties. *Construction and Building Materials*, **125**, 241–352.

Nagaraj H.B., Sravan M.V., Arun T.G. & Jagadish K.S. (2014) Role of lime with cement in long-term strength of compressed stabilized earth blocks. *International Journal of Sustainable Built Environment*, **3**, 54–61.

Namduri H. & Nasrazadani S. (2008) Quantitative analysis of iron oxides using Fourier transform infrared spectrophotometry. *Corrosion Science*, **50**, 2493–2497.

Ozturk S., Sutcu M., Erdogmus E. & Gencel O. (2019) Influence of tea waste concentration in the physical, mechanical and thermal properties of brick clay mixtures. *Construction and Building Materials*, **217**, 592–599.

Phonphuak N., Kanyakam S. & Chindaprasirt P. (2016) Utilization of waste glass to enhance physical–mechanical properties of fired clay brick. *Journal of Cleaner Production*, **112**, 3057–3062.

Pitak I., Baltušnikas A., Kalpokaitė-Dičkuvienė R., Kriukiene R. & Denafas G. (2022) Experimental study effect of bottom ash and temperature of firing on the properties, microstructure and pore size distribution of clay bricks: a Lithuania point of view. *Case Studies in Construction Materials*, **17**, e01230.

Rashid K., Haq E.U., Kamran M.S., Munir N., Shahid A. & Hanif I. (2019) Experimental and finite element analysis on thermal conductivity of burnt clay bricks reinforced with fibers. *Construction and Building Materials*, **221**, 190–199.

Rashid M.I., Benhelal E. & Rafiq S. (2020) Reduction of greenhouse gas emissions from gas, oil, and coal power plants in Pakistan by carbon capture and storage (CCS): a review. *Chemical Engineering and Technology*, **43**, 2140–2148.

Raut A.N. & Gomez C.P. (2017) Development of thermally efficient fibre-based eco-friendly brick reusing locally available waste materials. *Construction and Building Materials*, **133**, 275–284.

Ravisankar R., Kiruba S., Eswaran P., Senthilkumar G. & Chandrasekaran A. (2010) Mineralogical characterization studies of ancient potteries of Tamilnadu, India by FT-IR spectroscopic technique. *E-Journal of Chemistry*, **7**, 185–190.

Rizov B. (2012) Phase transformations from goethite to hematite and thermal decomposition in various nickeliferous laterite ores. *Journal of the University of Chemical Technology and Metallurgy*, **47**, 207–210.

Sedmale G., Sperberga I., Sedmalis U. & Valancius Z. (2006) Formation of high-temperature crystalline phases in ceramic from illite clay and dolomite. *Journal of the European Ceramic Society*, **26**, 3351–3355.

Semiz B. (2017) Characteristics of clay-rich raw materials for ceramic applications in Denizli region (western Anatolia). *Applied Clay Science*, **137**, 83–93.

Shi J., Chun Q., Mi Z., Feng S., Liu C., Liu Z. *et al.* (2023) Comparative study on material properties of ancient fired clay bricks of China. *Case Studies in Construction Materials*, **19**, e02463.

Slimanou H., Eliche-Quesada D., Kherbache S., Bouzidi N. & Tahakourt A.K. (2020) Harbor dredged sediment as raw material in fired clay brick production: characterization and properties. *Journal of Building Engineering*, **28**, 101085.

Souza C., Vieira C.M.F. & Monteiro S. (2008) Alterações microestruturais de cerâmica argilosa incorporada com rejeito de minério de ferro/Microstructural changes of clayey ceramic incorporated with iron ore tailings. *Revista Matéria*, **13**, 194–202.

Sutcu M., Alptekin H., Erdogmus E., Er Y. & Gencel O. (2015) Characteristics of fired clay bricks with waste marble powder addition as building materials. *Construction and Building Materials*, **82**, 1–8.

Sutcu M., Ozturk S., Yalamac E. & Gencel O. (2016) Effect of olive mill waste addition on the properties of porous fired clay bricks using Taguchi method. *Journal of Environmental Management*, **181**, 185–192.

Sutcu M., Erdogmus E., Gencel O., Gholampour A., Atan E. & Ozbakkaloglu T. (2019) Recycling of bottom ash and fly ash wastes in eco-friendly clay brick production. *Journal of Cleaner Production*, **233**, 753–764.

https://doi.org/10.1180/clm.2025.10015 Published online by Cambridge University Press

Terra F.S., Demattê J.A.M. & Viscarra Rossel R.A. (2015) Spectral libraries for quantitative analyses of tropical Brazilian soils: comparing vis-NIR and mid-IR reflectance data. *Geoderma*, **255–256**, 81–93.

Thejas H.K. & Hossiney N. (2022) Alkali-activated bricks made with mining waste iron ore tailings. *Case Studies in Construction Materials*, **16**, e00973.

Thomas G., Isabelle C., Frederic H., Catherine P. & Marie-Anne B. (2021) Demonstrating the influence of sediment source in dredged sediment recovery for brick and tile production. *Resources, Conservation and Recycling*, **171**, 105653.

US EPA. (1996) Method 3050B: Acid Digestion of Sludges, Sediments, and Soils, Revision 2. United States Environmental Protection Agency, Washington, DC, USA. Retrieved from https://www.epa.gov/sites/production/files/2015-06/documents/epa-3050b.pdf

Velasco P.M., Ortiz M.P.M., Giró M.A.M., Melia D.M. & Rehbein J.H. (2015) Development of sustainable fired clay bricks by adding kindling from vine shoot: study of thermal and mechanical properties. *Applied Clay Science*, **107**, 156–164.

Vilela A.P., Eugênio T.M.C., de Oliveira F.F., Mendes J.F., Ribeiro A.G.C., Brandão Vaz L.E.V.d.S. & Mendes R.F. (2020) Technological properties of soil–cement bricks produced with iron ore mining waste. *Construction and Building Materials*, **262**, 120883.

Wang C., Wang J., Li Q., Xu S. & Yang J. (2024) A review on recent development of foam ceramics prepared by particle-stabilized foaming technique. *Advances in Colloid and Interface Science*, **330**, 103198.

Weishi L., Guoyuan L., Ya X. & Qifei H. (2018) The properties and formation mechanisms of eco-friendly brick building materials fabricated from low-silicon iron ore tailings. *Journal of Cleaner Production*, **204**, 685–692.

Xin Y., Kurmus H., Mohajerani A., Dallol Y., Lao Y., Robert D. *et al.* (2021) Recycling crushed waste beer bottle glass in fired clay bricks. *Buildings*, **11**, 483.

Xin Y., Robert D., Mohajerani A., Tran P. & Pramanik B.K. (2023a) Utilizing rejected contaminants from the paper recycling process in fired clay brick production. *Construction and Building Materials*, **409**, 134031.

Xin Y., Robert D., Mohajerani A., Tran P. & Pramanik B.K. (2023b) A viable solution for industrial waste ash: recycling in fired clay bricks. *Journal of Materials in Civil Engineering*, **35**, 04023246.

Yang C., Cui C., Qin J. & Cui X. (2014) Characteristics of the fired bricks with low-silicon iron tailings. *Construction and Building Materials*, **70**, 36–42.

Zhang N., Tang B. & Liu X. (2021) Cementitious activity of iron ore tailing and its utilization in cementitious materials, bricks and concrete. *Construction and Building Materials*, **288**, 123022.

https://doi.org/10.1180/clm.2025.10015 Published online by Cambridge University Press